

Information-geometry-driven graph sequential growth

Harry T. BOND* Bertrand GAUTHIER* Kirstin STROKORB†

Abstract

We investigate the properties of a class of regularisation-free approaches for Gaussian graphical inference based on the information-geometry-driven sequential growth of initially edgeless graphs. Relating the growth of a graph to a coordinate descent process, we characterise the fully-corrective descents corresponding to information-optimal growths, and propose numerically efficient strategies for their approximation. We demonstrate the ability of the proposed procedures to reliably extract sparse graphical models while limiting the number of false detections, and illustrate how activation ranks can provide insight into the informational relevance of edge sets. The considered approaches are tuning-parameter-free and have complexities akin to coordinate descents.

Keywords: Gaussian graphical model, information geometry, coordinate descent, sequential inference, stability selection.

Mathematics Subject Classification: 62H22, 62B11, 90C25.

Contents

| | | |
|----------|--|-----------|
| 1 | Introduction | 2 |
| 2 | Framework and notations | 3 |
| 2.1 | Gaussian graphical loss | 3 |
| 2.2 | Coordinate directions and graph likelihood | 5 |
| 3 | Information-optimal graph sequential growth | 6 |
| 4 | Coordinate descent and graph optimality | 7 |
| 4.1 | Exact block update | 7 |
| 4.2 | Graph-optimal matrix approximation | 8 |
| 5 | Relaxed graph sequential growth | 9 |
| 6 | Experiments | 10 |
| 6.1 | Synthetic example based on 494_bus | 11 |
| 6.2 | Fully-synthetic simulation study | 14 |
| 6.3 | Recovering a gene network: the Riboflavin data | 15 |
| 7 | Concluding discussion | 18 |
| A | Proofs and technical results | 19 |

*Cardiff University, School of Mathematics — BondH@cardiff.ac.uk, GauthierB@cardiff.ac.uk

†University of Bath, Department of Mathematical Sciences — KS3047@bath.ac.uk

1 Introduction

Let \mathbf{x} be a d -dimensional centred Gaussian random vector with covariance $\boldsymbol{\Sigma}$ and precision $\boldsymbol{\Theta} = \boldsymbol{\Sigma}^{-1}$. When the matrix $\boldsymbol{\Theta}$ is sparse, the primary goal of graphical inference is to recover its sparsity pattern from the observation of independent realisations of \mathbf{x} . This task is often referred to as *graph recovery* or *structure learning* and is akin to learning the graph defined by the non-zero off-diagonal entries of $\boldsymbol{\Theta}$; this graph describes the *conditional independence structure* of \mathbf{x} ; see e.g. [25, 37]. Intrinsically related is the complementary task of *parameter learning*, that is, estimating the values of the non-null entries of $\boldsymbol{\Theta}$, see for instance [18]. More generally, practical motivation may stem from identifying sparse approximations of not-necessarily-sparse precision matrices. There exists a rich literature on graphical model estimation and we refer the reader to [10, 17, 35, 37] for overviews of major developments. Established techniques include partial-correlation testing, penalised likelihood maximisation, or neighbourhood selection [11, 30, 40].

Likelihood-based approaches for Gaussian graphical inference relate to the minimisation of convex functions of the form

$$f_{\mathbf{S}} : \mathbf{Q} \mapsto \text{trace}(\mathbf{S}\mathbf{Q}) - \log(\det(\mathbf{Q})), \quad \mathbf{Q} \in \mathcal{S}_{>0}^d,$$

with $\mathcal{S}_{>0}^d$ the convex cone of all order- d symmetric positive-definite matrices, and where \mathbf{S} is typically the sample covariance of the observations. We call $f_{\mathbf{S}}$ the *Gaussian graphical loss* with respect to \mathbf{S} ; see Section 2 for details. Graphical inference is in this case carried out by searching for sparse approximations of the argument of the minimum of $f_{\mathbf{S}}$. In graphical-lasso-type approaches [1, 12, 40], this is achieved by minimising $f_{\mathbf{S}}$ in combination with a sparsity-inducing regularisation term. A common approach is to minimise

$$\mathbf{Q} \mapsto f_{\mathbf{S}}(\mathbf{Q}) + \lambda \|\mathbf{Q}\|_{\ell^1}, \quad \mathbf{Q} \in \mathcal{S}_{>0}^d,$$

with $\lambda \geq 0$ and where $\|\mathbf{Q}\|_{\ell^1} = \sum_{i \neq j} |\mathbf{Q}_{i,j}|$ penalises the magnitude of the off-diagonal entries of \mathbf{Q} . Regularisation-based techniques enjoy very elegant properties and have been extensively studied in the literature; cf. also [5, 16, 29, 39]. In practice, they however require to appropriately tune the regularisation term, and they can sometimes lead to relatively high ratios of false detections [20, 22, 28]; see also Section 6 for illustrations.

In this work, we investigate the properties of a class of regularisation-free approaches for graphical inference based on the direct minimisation of $f_{\mathbf{S}}$ via information-geometry-driven coordinate descents with optimal diagonal initialisations. We leverage the analogy between edge activation and coordinate update, and characterise the descent corresponding to the likelihood-optimal growth of an initially edgeless graph. Specifically, optimal growths correspond to *fully-corrective* coordinate descents with *best-fully-corrective-improvement* selection rule (see Section 3). We then discuss numerically efficient strategies for the approximation of such descents, relying on approximate full correction (Section 4) and relaxed edge activation rules (Section 5).

The efficacy of the considered inference strategies is assessed on a comprehensive series of synthetic examples (Section 6), thereby demonstrating the ability of the considered growth-based approaches to reliably extract sparse graphs while limiting the number of false detections. We also illustrate how the proposed strategies can assist the estimation of graphical models in practical situations. General comments and further considerations are gathered in a concluding discussion (Section 7).

From a theoretical standpoint, the presented developments bring together classical results from probability, statistics and convex optimisation; to this extent, the contribution of this work is mostly methodological, describing the theoretical foundations of the proposed approaches and demonstrating the practical interest of sequential-growth-based procedures as diagnostic tools for graphical-model estimation. For completeness, proofs of all the results stated in the main body of the paper are presented in Appendix A.

2 Framework and notations

Throughout this note, we use the classical matrix notation and identify a vector $\mathbf{x} \in \mathbb{R}^d$, $d \in \mathbb{N}$, as the $d \times 1$ column matrix defined by the coefficients of \mathbf{x} in the canonical basis $\{\mathbf{e}_i\}_{i \in [d]}$ of \mathbb{R}^d ; $[d]$ stands for the set of all integers between 1 and d . The transpose of a matrix \mathbf{M} is denoted by \mathbf{M}^T , and \mathbf{I}_d is the $d \times d$ identity matrix; $\|\mathbf{M}\|_F$ stands for the Frobenius norm of \mathbf{M} , and the underlying inner product is denoted by $\langle \cdot | \cdot \rangle_F$. Let $\mathcal{M}^d = \mathbb{R}^{d \times d}$ be the linear space of all d -order matrices; we consider the usual topology on \mathcal{M}^d . The linear subspaces of all diagonal and all symmetric matrices are denoted by \mathcal{D}^d and \mathcal{S}^d , respectively. Further, $\mathcal{S}_{\geq 0}^d$ and $\mathcal{S}_{>0}^d$ stand for the convex cones of all symmetric positive-semidefinite and symmetric positive-definite matrices of order d , respectively. For $\mathcal{K} \subseteq \mathcal{S}_{>0}^d$, we set

$$\lambda_{\min}(\mathcal{K}) = \inf \{\lambda_{\min}(\mathbf{Q}) \mid \mathbf{Q} \in \mathcal{K}\} \quad \text{and} \quad \lambda_{\max}(\mathcal{K}) = \sup \{\lambda_{\max}(\mathbf{Q}) \mid \mathbf{Q} \in \mathcal{K}\},$$

where $\lambda_{\min}(\mathbf{Q})$ and $\lambda_{\max}(\mathbf{Q})$ are the smallest and largest eigenvalues of \mathbf{Q} , respectively. We also set $\mathbb{N}_0 = \mathbb{N} \cup \{0\}$.

2.1 Gaussian graphical loss

Consider a d -dimensional centred Gaussian random vector $\mathbf{x} \sim \mathcal{N}_{\Sigma}$, with $\Sigma \in \mathcal{S}_{>0}^d$. Let $(\mathbf{x}_l)_{l \in [n]}$ be $n \in \mathbb{N}$ independent realisations of \mathbf{x} . The negative log-likelihood of $\mathbf{Q} \in \mathcal{S}_{>0}^d$ being the precision of \mathbf{x} reads

$$-\ell(\mathcal{N}_{\mathbf{Q}^{-1}} \mid \mathbf{x}_1, \dots, \mathbf{x}_n) = \frac{n}{2} [\text{trace}(\hat{\Sigma}\mathbf{Q}) - \log(\det(\mathbf{Q})) + d \log(2\pi)], \quad (1)$$

with $\hat{\Sigma} = \frac{1}{n} \sum_{l=1}^n \mathbf{x}_l \mathbf{x}_l^T \in \mathcal{S}_{\geq 0}^d$ the classical biased estimate of Σ . More generally, we call

$$f_{\mathbf{S}} : \mathcal{S}_{>0}^d \rightarrow \mathbb{R}, \quad f_{\mathbf{S}}(\mathbf{Q}) = \text{trace}(\mathbf{S}\mathbf{Q}) - \log(\det(\mathbf{Q}))$$

the *Gaussian graphical loss* with respect to $\mathbf{S} \in \mathcal{S}_{\geq 0}^d$; see Remark 2.1 for an information geometric interpretation of the map $f_{\mathbf{S}}$.

Observing that \mathcal{S}^d is the tangent space of $\mathcal{S}_{>0}^d$ at any given $\mathbf{Q} \in \mathcal{S}_{>0}^d$, the first and second total derivatives of $f_{\mathbf{S}}$ at $\mathbf{Q} \in \mathcal{S}_{>0}^d$ read

$$D_{\mathbf{Q}} f_{\mathbf{S}} : \mathbf{H} \mapsto \text{trace}((\mathbf{S} - \mathbf{Q}^{-1})\mathbf{H}) = \langle \mathbf{S} - \mathbf{Q}^{-1} \mid \mathbf{H} \rangle_F, \quad \mathbf{H} \in \mathcal{S}^d, \text{ and}$$

$$D_{\mathbf{Q}}^2 f_{\mathbf{S}} : (\mathbf{H}_1, \mathbf{H}_2) \mapsto \text{trace}(\mathbf{Q}^{-1}\mathbf{H}_1\mathbf{Q}^{-1}\mathbf{H}_2) = \langle \mathbf{H}_1\mathbf{Q}^{-1} \mid \mathbf{Q}^{-1}\mathbf{H}_2 \rangle_F, \quad \mathbf{H}_1 \text{ and } \mathbf{H}_2 \in \mathcal{S}^d.$$

In particular, $f_{\mathbf{S}}$ is continuous over $S_{>0}^d$. Lemma 2.1 below recalls some important properties of the map $f_{\mathbf{S}}$. We say that a function $f : S_{>0}^d \rightarrow \mathbb{R}$ is *coercive*¹ if for any sequence $(\mathbf{Q}_k)_{k \in \mathbb{N}} \subset S_{>0}^d$ such that $\lambda_{\min}(\mathbf{Q}_k) \rightarrow 0$ or $\lambda_{\max}(\mathbf{Q}_k) \rightarrow +\infty$, we have $f(\mathbf{Q}_k) \rightarrow +\infty$. If f is also continuous, then its sublevel sets are compact.

Lemma 2.1. *For all $\mathbf{S} \in S_{\geq 0}^d$, the map $f_{\mathbf{S}}$ is strictly convex on $S_{>0}^d$. If \mathbf{S} is invertible, then $f_{\mathbf{S}}$ is coercive over $S_{>0}^d$ and is minimised at $\mathbf{Q} = \mathbf{S}^{-1}$. If \mathbf{S} is singular, then $f_{\mathbf{S}}$ is unbounded from below.*

Let $\nabla f_{\mathbf{S}}(\mathbf{Q}) = \mathbf{S} - \mathbf{Q}^{-1}$ be the gradient of $f_{\mathbf{S}}$ at $\mathbf{Q} \in S_{>0}^d$ with respect to the Frobenius inner product. Lemma 2.2 expresses that the map $f_{\mathbf{S}}$ is strongly convex and has Lipschitz-continuous gradient on any non-empty compact convex subset of $S_{>0}^d$.

Lemma 2.2. *Let $\mathbf{S} \in S_{\geq 0}^d$. If $\mathcal{K} \subset S_{>0}^d$ is such that $\lambda_{\min}(\mathcal{K}) > 0$, then we have*

$$\|\nabla f_{\mathbf{S}}(\mathbf{Q}_1) - \nabla f_{\mathbf{S}}(\mathbf{Q}_2)\|_{\text{F}} \leq \|\mathbf{Q}_1 - \mathbf{Q}_2\|_{\text{F}} / \lambda_{\min}^2(\mathcal{K}), \quad \mathbf{Q}_1 \text{ and } \mathbf{Q}_2 \in \mathcal{K}.$$

If $\mathcal{K} \subset S_{>0}^d$ is such that $\lambda_{\max}(\mathcal{K})$ is finite, then we have

$$\langle \nabla f_{\mathbf{S}}(\mathbf{Q}_1) - \nabla f_{\mathbf{S}}(\mathbf{Q}_2) | \mathbf{Q}_1 - \mathbf{Q}_2 \rangle_{\text{F}} \geq \|\mathbf{Q}_1 - \mathbf{Q}_2\|_{\text{F}}^2 / \lambda_{\max}^2(\mathcal{K}), \quad \mathbf{Q}_1 \text{ and } \mathbf{Q}_2 \in \mathcal{K}.$$

In view of Lemma 2.1, the negative log-likelihood (1) admits a minimum over $S_{>0}^d$ solely when $\hat{\Sigma}$ is invertible. In situations where $\hat{\Sigma}$ is singular (for $n \leq d$ for instance), it is common to introduce a *ridge penalty* and consider the graphical loss defined by $\mathbf{S} = \hat{\Sigma} + \mathbf{T}$, with $\mathbf{T} \in S_{>0}^d$. A typical instance is to use $\mathbf{T} = \gamma^2 \mathbf{I}_d$, with $\gamma > 0$ (Gaussian observation noise); see for instance [13, 38]. A ridge penalty can also help to improve numerical stability or to account for account measurement errors.

Remark 2.1. The loss function $f_{\mathbf{S}}$ is closely related to the information geometry of multivariate Gaussian distributions, which dates back to the works of [6, 21, 36]. Following for instance [8], the Gaussian graphical loss can be recovered from the *scoring rule*

$$\mathbf{S}(\mathbf{x}, \mathcal{N}_{\mathbf{Q}^{-1}}) = \mathbf{x}^T \mathbf{Q} \mathbf{x} - \log(\det(\mathbf{Q})), \quad \mathbf{x} \in \mathbb{R}^d \text{ and } \mathbf{Q} \in S_{>0}^d.$$

When \mathbf{S} is invertible, we have

$$f_{\mathbf{S}}(\mathbf{Q}) - f_{\mathbf{S}}(\mathbf{S}^{-1}) = \text{trace}(\mathbf{S} \mathbf{Q} - \mathbf{I}_d) - \log(\det(\mathbf{S} \mathbf{Q})) = 2D_{\text{KL}}(\mathcal{N}_{\mathbf{S}} \| \mathcal{N}_{\mathbf{Q}^{-1}}),$$

with $D_{\text{KL}}(\mathcal{N}_{\mathbf{S}} \| \mathcal{N}_{\mathbf{Q}^{-1}})$ the *Kullback-Leibler divergence* from $\mathcal{N}_{\mathbf{Q}^{-1}}$ to $\mathcal{N}_{\mathbf{S}}$. Here, the value $f_{\mathbf{S}}(\mathbf{S}^{-1}) = d + \log(\det(\mathbf{S}))$ is the *generalised entropy* or *information measure* of the distribution $\mathcal{N}_{\mathbf{S}}$. \triangleleft

¹We use the term *coercive* for convenience to encapsulate the idea of growing to $+\infty$ when reaching the boundary of the domain $S_{>0}^d$.

2.2 Coordinate directions and graph likelihood

For i and $j \in [d]$, $i < j$, let

$$\mathbf{B}(i, i) = \mathbf{e}_i \mathbf{e}_i^T \quad \text{and} \quad \mathbf{B}(i, j) = [\mathbf{e}_i \mathbf{e}_j^T + \mathbf{e}_j \mathbf{e}_i^T] / \sqrt{2},$$

so that the collection $\mathcal{B} = \{\mathbf{B}(i, j) \mid 1 \leq i < j \leq d\}$ forms an orthonormal basis of S^d for the Frobenius inner product. When minimising $f_{\mathbf{S}}$, a line search along $\mathbf{B}(i, i)$ updates the i -th diagonal entry of the current iterate (*diagonal update*), while a line search along $\mathbf{B}(i, j)$ updates the (i, j) -entry and its symmetric counterpart (*off-diagonal update*). We denote by

$$\mathcal{D} = \{(i, i)\}_{i \in [d]} \quad \text{and} \quad \mathcal{U} = \{(i, j)\}_{1 \leq i < j \leq d}$$

the sets of all diagonal and upper-diagonal indices of a $d \times d$ matrix, respectively.

We use the following terminology to make the connections between graph sequential growth strategies and associated coordinate descents precise. For $\mathbf{Q} \in S_{>0}^d$, the *support* (or *activation*) $\text{supp}(\mathbf{Q})$ of \mathbf{Q} is given by

$$\text{supp}(\mathbf{Q}) = \{(i, j) \in \mathcal{D} \cup \mathcal{U} \mid \mathbf{Q}_{i,j} \neq 0\}.$$

Observe that we always have $\mathcal{D} \subseteq \text{supp}(\mathbf{Q})$. The set of upper-diagonal indices We refer to

$$\text{edge}(\mathbf{Q}) = \text{supp}(\mathbf{Q}) \cap \mathcal{U} \quad \text{and} \quad \text{free}(\mathbf{Q}) = \mathcal{U} \setminus \text{edge}(\mathbf{Q}),$$

as the *edge set defined by \mathbf{Q}* and the *free set of \mathbf{Q}* . Naturally, $\text{edge}(\mathbf{Q})$ defines the edge set of a simple d -vertex undirected graph. We say that a matrix $\mathbf{Q} \in S_{>0}^d$ is *supported by a graph $G = ([d], \mathcal{E})$* if $\text{edge}(\mathbf{Q}) \subseteq \mathcal{E}$, where $\mathcal{E} \subseteq \mathcal{U}$ is the edge set of G .

For $\mathbf{S} \in S_{\geq 0}^d$ and $G = ([d], \mathcal{E})$, $\mathcal{E} \subseteq \mathcal{U}$, the *Gaussian graphical loss* $\tilde{f}_{\mathbf{S}}(G)$ of the graph G with respect to \mathbf{S} is the infimum of $f_{\mathbf{S}}$ over the set of all symmetric positive definite matrices supported by G , that is,

$$\begin{aligned} \tilde{f}_{\mathbf{S}}(G) &= \inf \{f_{\mathbf{S}}(\mathbf{Q}) \mid \mathbf{Q} \in S_{>0}^d, \text{edge}(\mathbf{Q}) \subseteq \mathcal{E}\} \\ &= \inf \{f_{\mathbf{S}}(\mathbf{Q}) \mid \mathbf{Q} \in \text{span}\{\mathbf{B}(i, j) \mid (i, j) \in \mathcal{D} \cup \mathcal{E}\} \cap S_{>0}^d\}. \end{aligned} \tag{2}$$

For $\mathbf{S} \in S_{\geq 0}^d$ such that $\text{diag}(\mathbf{S}) \in \mathbb{R}_{>0}^d$, the graphical loss of the edgeless graph $G_{\emptyset} = ([d], \emptyset)$ is realised by the diagonal matrix $\mathbf{Q}_{\mathbf{S}, \emptyset} \in \mathcal{D}^d \cap S_{>0}^d$, with

$$[\mathbf{Q}_{\mathbf{S}, \emptyset}]_{i,i} = 1/\mathbf{S}_{i,i}, \quad i \in [d]. \tag{3}$$

Indeed, we have $[\nabla f_{\mathbf{S}}(\mathbf{Q}_{\mathbf{S}, \emptyset})]_{i,i} = 0$, $i \in [d]$, and so $\tilde{f}_{\mathbf{S}}(G_{\emptyset}) = f_{\mathbf{S}}(\mathbf{Q}_{\mathbf{S}, \emptyset})$. More generally, when \mathbf{S} is invertible, the infimum appearing in (2) is always a minimum.

Lemma 2.3. *Let $\mathbf{S} \in S_{>0}^d$. For $G = ([d], \mathcal{E})$, $\mathcal{E} \subseteq \mathcal{U}$, there exists a unique matrix $\mathbf{Q}_{\mathbf{S}, \mathcal{E}} \in S_{>0}^d$ such that $\text{edge}(\mathbf{Q}) \subseteq \mathcal{E}$ and $\tilde{f}_{\mathbf{S}}(G) = f_{\mathbf{S}}(\mathbf{Q}_{\mathbf{S}, \mathcal{E}})$. We have $[\nabla f_{\mathbf{S}}(\mathbf{Q}_{\mathbf{S}, \mathcal{E}})]_{i,j} = 0$ for all $(i, j) \in \mathcal{D} \cup \mathcal{E}$.*

For a general graph $G = ([d], \mathcal{E})$, an analytical expression for the minimising matrix $\mathbf{Q}_{\mathbf{S}, \mathcal{E}}$ does not exist. The properties of such matrices, and algorithms for their approximation, are for instance presented in [37], an early key reference on relevant matrix completions being [36]; see also Section 4. We refer to $\mathbf{Q}_{\mathbf{S}, \mathcal{E}}$ as the *graph-optimal matrix for \mathbf{S} and G* .

3 Information-optimal graph sequential growth

We use the term *graph sequential growth* for the process of sequentially adding edges to an initially edgeless graph, the vertex set $[d]$ staying fixed. Since a sequential growth corresponds to the definition of a *total order* on the set of upper-diagonal indices \mathcal{U} , setting $M = \text{card}(\mathcal{U}) = d(d - 1)/2$, we can equivalently identify a graph sequential growth with the specification of a finite sequence $\{(i, j)^{(k)}\}_{k=1}^M$ of distinct edges. We denote the underlying graphs as

$$G^{(0)} = ([d], \emptyset), \quad \text{and} \quad G^{(k)} = ([d], \mathcal{E}^{(k)}), \quad \text{with} \quad \mathcal{E}^{(k)} = \{(i, j)^{(l)}\}_{l=1}^k, k \in [M].$$

Observe that $\text{card}(\mathcal{E}^{(k)}) = k$ and $\mathcal{E}^{(M)} = \mathcal{U}$. Graph-sequential growths corresponds to forward-search methods, see for instance [1]. We refer to the operation of adding an edge to a current graph as *edge activation*.

Definition 3.1. A sequence of distinct edges $\{(i, j)^{(k)}\}_{k=1}^M$ defines an information-optimal graph sequential growth for $\mathbf{S} \in \mathcal{S}_{>0}^d$ if for all $k \in [M]$, we have

$$\tilde{f}_{\mathbf{S}}(G^{(k)}) = \min \left\{ \tilde{f}_{\mathbf{S}}(G) \mid G = ([d], \mathcal{E}^{(k-1)} \cup \{(i, j)\}), (i, j) \in \mathcal{U} \setminus \mathcal{E}^{(k-1)} \right\}.$$

If $\{(i, j)^{(k)}\}_{k=1}^M$ defines an information-optimal graph sequential growth for $\mathbf{S} \in \mathcal{S}_{>0}^d$, then the underlying sequence of graph-optimal matrices $\{\mathbf{Q}_{\mathbf{S}, \mathcal{E}^{(k)}}\}_{k=0}^M$ corresponds to the iterates of a coordinate descent for the minimisation of $f_{\mathbf{S}}$, with *optimal diagonal initialisation, fully-corrective update rule*, and *best-fully-corrective-improvement (BFCI) selection rule*; as detailed in Algorithm 1 and the subsequent discussion.

For $\mathbf{Q} \in \mathcal{S}_{>0}^d$ and $(i, j) \in \mathcal{U}$, define the *fully-corrective improvement score*

$$\mathcal{I}_{\mathbf{S}}^{\text{FC}}(\mathbf{Q}, (i, j)) = f_{\mathbf{S}}(\mathbf{Q}) - \tilde{f}_{\mathbf{S}}(G), \quad \text{with} \quad G = ([d], \text{edge}(\mathbf{Q}) \cup \{(i, j)\}).$$

Note that for $G = ([d], \mathcal{E})$ and $(i, j) \in \mathcal{E}$, we have $\mathcal{I}_{\mathbf{S}}^{\text{FC}}(\mathbf{Q}_{\mathbf{S}, \mathcal{E}}, (i, j)) = 0$.

Algorithm 1: Information-optimal graph sequential growth.

given $\mathbf{S} \in \mathcal{S}_{>0}^d$.

Set $\mathbf{Q}^{(0)} = \mathbf{Q}_{\mathbf{S}, \emptyset}$ and $\mathcal{E}^{(0)} = \emptyset$ (initialisation, see (3) above).

for $k \in [M]$ do

1. Compute $(i, j)^{(k)} \in \arg \max \left\{ \mathcal{I}_{\mathbf{S}}^{\text{FC}}(\mathbf{Q}^{(k-1)}, (i, j)) \mid (i, j) \in \text{free}(\mathbf{Q}^{(k-1)}) \right\}$.
2. Set $\mathcal{E}^{(k)} = \mathcal{E}^{(k-1)} \cup \{(i, j)^{(k)}\}$ and $\mathbf{Q}^{(k)} = \mathbf{Q}_{\mathbf{S}, \mathcal{E}^{(k)}}$.

return $\{(i, j)^{(k)}\}_{k \in [M]}$.

The interpretation of Algorithm 1 as a coordinate descent with fully-corrective update follows from observing that for $k \in [M]$, we have

$$f_{\mathbf{S}}(\mathbf{Q}^{(k)}) = \min \left\{ f_{\mathbf{S}}(\mathbf{Q}) \mid \mathbf{Q} \in \text{span} \left\{ \mathbf{B}(i, j) \mid (i, j) \in \text{supp}(\mathbf{Q}^{(k-1)}) \cup \{(i, j)^{(k)}\} \right\} \right\}.$$

In addition to $\mathbf{B}(i, j)^{(k)}$ and the diagonal coordinate directions $\mathbf{B}(i, i)$, $i \in [d]$, for $k \geq 2$, the computation of the iterate $\mathbf{Q}^{(k)}$ therefore also involves all the previously activated off-diagonal directions $\mathbf{B}(i, j)^{(l)}$, $l \in [k-1]$. The selection rule in Algorithm 1 amounts to

selecting the edge leading to the best fully-corrective improvement, that is, the maximum improvement after full correction.

As mentioned in Section 2.2, for a general graph $G = ([d], \mathcal{E})$, it is generally not possible to obtain precisely the graph-optimal matrix $\mathbf{Q}_{S, \mathcal{E}}$ (let alone in exact arithmetic), and one needs instead to rely on iterative approximation procedures; see Section 4. Moreover, for a current iterate $\mathbf{Q}^{(k-1)}$, the characterisation of the optimal edge $(i, j)^{(k)}$ involves the computation of $M - k + 1$ such matrices. From a numerical standpoint, the execution of Algorithm 1 is thus computationally prohibitive, especially when the dimension d is large; this limitation is generally inherent to forward-backward searches [1, 37]. A natural alternative is to consider coordinate descents with relaxed selection and update rules as discussed in Section 5. In practice, one might not necessarily compute a sequential growth in full, and instead stop the growth procedure once a maximum number of edges k_{\max} is reached (partial growth).

4 Coordinate descent and graph optimality

In this section, we discuss the minimisation of f_S , $S \in S_{>0}^d$, over the convex cone of all symmetric positive-definite matrices supported by a given graph, that is, the approximation of matrices of the form $\mathbf{Q}_{S, \mathcal{E}}$, $\mathcal{E} \subseteq \mathcal{U}$. More specifically, we consider exact group-coordinate descents that consist of either updating a diagonal entry of the current iterate, or one of its 2×2 principal submatrices; we refer to such updates as $\{1, 2\}$ -updates (see Section 4.1).

4.1 Exact block update

The Gaussian loss f_S can be minimised via exact coordinate descent, that is, by performing exact line searches along directions in the set of coordinate directions \mathcal{B} (see Section 2.2). It is nevertheless also possible to characterise exact group-coordinate updates by directly updating a principal submatrix of the current iterate, as described in Lemma 4.1 (see for instance [36, Lemma 2], and also [14, 25]).

Lemma 4.1 (exact order- m update). *Consider $\mathbf{Q} \in S_{>0}^d$ and let $I \subseteq [d]$ be a subset of size m ; set $\mathbf{R} = \mathbf{Q}^{-1}$. The minimum of f_S over $(\mathbf{Q} + \text{span}\{\mathbf{B}(i, j) \mid i, j \in I, i \leq j\}) \cap S_{>0}^d$ is reached at $\tilde{\mathbf{Q}} \in S_{>0}^d$, with*

$$\tilde{\mathbf{Q}}_{I,I} = \mathbf{Q}_{I,I} + (\mathbf{S}_{I,I})^{-1} - (\mathbf{R}_{I,I})^{-1} \quad \text{and} \quad \tilde{\mathbf{Q}}_{i,j} = \mathbf{Q}_{i,j} \quad \text{for } i \text{ or } j \notin I.$$

Setting $\tilde{\mathbf{R}} = \tilde{\mathbf{Q}}^{-1}$, we then have

$$\begin{pmatrix} \tilde{\mathbf{R}}_{I,I} & \tilde{\mathbf{R}}_{I,I^c} \\ \tilde{\mathbf{R}}_{I^c,I} & \tilde{\mathbf{R}}_{I^c,I^c} \end{pmatrix} = \begin{pmatrix} \mathbf{S}_{I,I} & \mathbf{S}_{I,I}(\mathbf{R}_{I,I})^{-1}\mathbf{R}_{I,I^c} \\ \mathbf{R}_{I^c,I}(\mathbf{R}_{I,I})^{-1}\mathbf{S}_{I,I} & \mathbf{R}_{I^c,I^c} - \mathbf{R}_{I^c,I}(\mathbf{R}_{I,I})^{-1}[\mathbf{I}_m - \mathbf{S}_{I,I}(\mathbf{R}_{I,I})^{-1}]\mathbf{R}_{I,I^c} \end{pmatrix},$$

and $f_S(\mathbf{Q}) - f_S(\tilde{\mathbf{Q}}) = \text{trace}(\mathbf{S}_{I,I}(\mathbf{R}_{I,I})^{-1}) - m - \log(\det(\mathbf{S}_{I,I}(\mathbf{R}_{I,I})^{-1}))$.

In Lemma 4.1, the case $I = \{i\}$, $i \in [d]$, describes an exact line search along $\mathbf{B}(i, i)$; we refer to such an update as a 1 -update (or *order-1 update*). The case $I = \{i, j\}$, $(i, j) \in \mathcal{U}$, corresponds to the simultaneous update of $\mathbf{Q}_{i,j}$, $\mathbf{Q}_{j,i}$, $\mathbf{Q}_{i,i}$ and $\mathbf{Q}_{j,j}$; we refer to such an

update as a *2-update* (or *order-2 update*). Higher order updates may also be considered; such updates relate to the existence of cliques in the underlying graphs, see for instance [36]. In what follows, we only consider $\{1, 2\}$ -*updates*, that is, order-1 or order-2 updates.

4.2 Graph-optimal matrix approximation

For $\mathbf{S} \in S_{>0}^d$ and $G = ([d], \mathcal{E})$, the following general procedure (Algorithm 2) produces sequences of iterates converging towards $\mathbf{Q}_{\mathbf{S}, \mathcal{E}}$. In the framework of Algorithm 1, Algorithm 2 can be used to approximate the full correction related to the activation of a given edge in the free set of a current iterate. In practice, the optimisation is carried out until a given stopping criterion is satisfied (see Remark 4.1 below); for numerical efficiency, rather than performing matrix inversion, one should use Lemma 4.1 to update the inverse of the current iterates.

Algorithm 2: Coordinate descent with $\{1, 2\}$ -updates and support restriction.

given $\mathbf{S} \in S_{>0}^d$, $G = ([d], \mathcal{E})$, and $\mathbf{Q}^{(0)} \in S_{>0}^d$ such that $\text{edge}(\mathbf{Q}^{(0)}) \subseteq \mathcal{E}$.

Set $t = 1$.

repeat

1. Select $(i, j)^{(t)} \in \mathcal{D} \cup \mathcal{E}$ (selection rules are discussed below).
2. Perform the corresponding $\{1, 2\}$ -update to define $\mathbf{Q}^{(t)}$ from $\mathbf{Q}^{(t-1)}$
(use Lemma 4.1 with $\mathbf{Q} = \mathbf{Q}^{(t-1)}$, $\mathbf{R} = (\mathbf{Q}^{(t-1)})^{-1}$ and $\tilde{\mathbf{Q}} = \mathbf{Q}^{(t)}$); increment t .

return $\{\mathbf{Q}^{(t)}\}_{t \in \mathbb{N}_0}$.

By construction, and independently of the selection rule considered, the sequence $\{f_{\mathbf{S}}(\mathbf{Q}^{(t)})\}_{t \in \mathbb{N}_0}$ is non-increasing and for all $t \in \mathbb{N}_0$ we have

$$\mathbf{Q}^{(t)} \in \{\mathbf{Q} \in S_{>0}^d \mid f_{\mathbf{S}}(\mathbf{Q}) \leq f_{\mathbf{S}}(\mathbf{Q}^{(0)}) \text{ and } \text{edge}(\mathbf{Q}) \subseteq \mathcal{E}\} = \mathcal{K}_{0, \mathcal{E}}.$$

By Lemma 2.1, $\mathcal{K}_{0, \mathcal{E}}$ is convex and compact (as it is the intersection of a convex compact sublevel set of $f_{\mathbf{S}}$ with a linear subspace of S^d). The strong-convexity of $f_{\mathbf{S}}$ and the Lipschitz-continuity of its gradient over $\mathcal{K}_{0, \mathcal{E}}$ (see Lemma 2.2) thus ensure the convergence of Algorithm 2 for a variety of selection rules, including the cyclic rule, the random-uniform rule, or various gradient-based rules; see for instance [3, 19, 32, 33] and references therein. The convergence is generally at-worst-linear, as shown below for the *Gauss-Southwell* (GS) selection rule, which consists of considering the coordinate directions

$$(i, j)^{(t)} \in \arg \max_{(i, j) \in \mathcal{D} \cup \mathcal{E}} |\langle \nabla f_{\mathbf{S}}(\mathbf{Q}^{(t-1)}) | \mathbf{B}(i, j) \rangle_{\mathbb{F}}|, \quad t \in \mathbb{N}.$$

Theorem 4.1. *For the GS selection rule, the sequence of iterates $\{\mathbf{Q}^{(t)}\}_{t \in \mathbb{N}_0}$ generated by Algorithm 2 satisfies*

$$f_{\mathbf{S}}(\mathbf{Q}^{(t)}) - f_{\mathbf{S}}(\mathbf{Q}_{\mathbf{S}, \mathcal{E}}) \leq \left(1 - \frac{\mu}{mL}\right)^t (f_{\mathbf{S}}(\mathbf{Q}^{(0)}) - f_{\mathbf{S}}(\mathbf{Q}_{\mathbf{S}, \mathcal{E}})), \quad t \in \mathbb{N}_0,$$

with $\mu = 1/\lambda_{\max}^2(\mathcal{K}_{0, \mathcal{E}})$, $L = 1/\lambda_{\min}^2(\mathcal{K}_{0, \mathcal{E}})$ and $m = \text{card}(\mathcal{D} \cup \mathcal{E})$.

Remark 4.1. In the framework of Theorem 4.1, we have (see (7) in Appendix A)

$$f_{\mathbf{S}}(\mathbf{Q}^{(t-1)}) - f_{\mathbf{S}}(\mathbf{Q}_{\mathbf{S}, \mathcal{E}}) \leq \frac{mL}{\mu} (f_{\mathbf{S}}(\mathbf{Q}^{(t-1)}) - f_{\mathbf{S}}(\mathbf{Q}^{(t)})), \quad t \in \mathbb{N},$$

which provides an (implicit) upper bound on the optimality gap based on the magnitude of the current improvement. Hence, one may decide to stop the descent once the current improvement reaches a given fraction of the initial one, that is, once the condition

$$f_{\mathbf{S}}(\mathbf{Q}^{(t-1)}) - f_{\mathbf{S}}(\mathbf{Q}^{(t)}) \leq \tau (f_{\mathbf{S}}(\mathbf{Q}^{(0)}) - f_{\mathbf{S}}(\mathbf{Q}^{(1)}))$$

is satisfied, with $0 < \tau \leq 1$. In our experiments of Section 6, we implement such a stopping rule in combination with an upper bound on the number of iterations of the form $\lceil \alpha m + \beta \rceil$, with α and $\beta \geq 0$; recall that $m = \text{card}(\mathcal{E})$. \triangleleft

5 Relaxed graph sequential growth

The information-optimal graph sequential growth for $\mathbf{S} \in \mathcal{S}_{>0}^d$ corresponds to a coordinate descent for the minimisation of $f_{\mathbf{S}}$ with fully-corrective update and BFCI selection rule (see Section 3). To mitigate the numerical cost inherent to such descents, relaxed selection and update rules may be considered. We focus on the ones below. Contrary to the BFCI rule, the presented rules do not involve the computation of graph-optimal matrices. Many variants of the described strategies could be considered.

Best block improvement (BBI). Following Lemma 4.1, for $\mathbf{Q} \in \mathcal{S}_{>0}^d$ and $(i, j) \in \mathcal{U}$, setting $\mathbf{R} = \mathbf{Q}^{-1}$ and $I = \{i, j\}$, we define the *block improvement score*

$$\mathcal{I}_{\mathbf{S}}^{\mathbf{B}}(\mathbf{Q}, (i, j)) = \text{trace}(\mathbf{S}_{I, I}(\mathbf{R}_{I, I})^{-1}) - 2 - \log(\det(\mathbf{S}_{I, I}(\mathbf{R}_{I, I})^{-1})).$$

The BBI selection rule consists of selecting the 2-update leading to the best improvement, without accounting for full correction, that is,

$$(i, j)^{(k)} \in \arg \max_{(i, j) \in \text{free}(\mathbf{Q}^{(k-1)})} \mathcal{I}_{\mathbf{S}}^{\mathbf{B}}(\mathbf{Q}^{(k-1)}, (i, j)).$$

Gauss-Southwell-Lipschitz (GSL). The GSL rule is a variant of the GS rule that also accounts for the local Lipschitz continuity of the gradient, see [33]; it is defined as

$$(i, j)^{(k)} \in \arg \max_{(i, j) \in \text{free}(\mathbf{Q}^{(k-1)})} (D_{\mathbf{Q}^{(k-1)}} f_{\mathbf{S}}(\mathbf{B}(i, j)))^2 / D_{\mathbf{Q}^{(k-1)}}^2 f_{\mathbf{S}}(\mathbf{B}(i, j), \mathbf{B}(i, j)).$$

Observe that $D_{\mathbf{Q}}^2 f_{\mathbf{S}}(\mathbf{B}(i, j), \mathbf{B}(i, j)) = \mathbf{R}_{i, i} \mathbf{R}_{j, j} + \mathbf{R}_{i, j}^2$, with $\mathbf{R} = \mathbf{Q}^{-1}$ and $(i, j) \in \mathcal{U}$. In terms of the amount of work, the GSL rule is less costly than the BBI rule. Note that the GSL and BBI selection rules can also be used in the framework of Algorithm 2.

Algorithm 3 below describes a general class of coordinate-descent-type strategies for graph sequential growth. The algorithm consists of two nested loops: the outer loop performs edge activation, and the inner loop uses Algorithm 2 to approximate full correction. Similarly to Algorithm 1, one might stop the procedure in practice once a maximum number of edges k_{\max} is reached (partial growth).

Algorithm 3: Relaxed graph sequential growth.

given $\mathbf{S} \in \mathcal{S}_{>0}^d$.

Set $\mathbf{Q}^{(0)} = \mathbf{Q}_{\mathbf{S}, \emptyset}$ and $\mathcal{E}^{(0)} = \emptyset$ (initialisation).

for $k \in [M]$ **do**

1. Select $(i, j)^{(k)} \in \text{free}(\mathbf{Q}^{(k-1)})$ (edge activation, see selection rules above), and set $\mathcal{E}^{(k)} = \mathcal{E}^{(k-1)} \cup \{(i, j)^{(k)}\}$.
2. Use Algorithm 2 initialised at $\mathbf{Q}^{(k-1)}$ to compute an approximation $\mathbf{Q}^{(k)}$ of $\mathbf{Q}_{\mathbf{S}, \mathcal{E}^{(k)}}$ (approximate full correction, see the stopping rule in Remark 4.1).

return $\{(i, j)^{(k)}\}_{k \in [M]}$.

In our experiments of Section 6, we also implement a variant of Algorithm 3 relying on approximate full corrections to approximate the BFCI selection rule. More precisely, we systematically use Algorithm 2 with the stopping rule discussed in Remark 4.1 to approximate the required graph-optimal matrices. In terms of amount of work and for identical stopping rules for approximate full correction, computing the full BFCI growth requires $M(M + 1)/2$ full corrections, whereas the full GSL or BBI growths involve only M full corrections.

6 Experiments

We illustrate the graph-recovery ability of the discussed strategies (Algorithm 3) on a series of examples. In Sections 6.1 and 6.2, we consider synthetic data and compare the proposed graph-sequential-growth procedures with graphical lasso (Glasso; see Remark 6.1), and with the naive sequential growths defined by the magnitude of the entries of the sample precision and partial-correlation matrices (see Remark 6.2). An application involving gene-expression data is presented in Section 6.3.

To ensure invertibility and for simplicity, we systematically add a ridge penalty to the sample covariance matrix and work with $\mathbf{S} = \hat{\Sigma} + \gamma^2 \mathbf{I}_d$, with $\gamma^2 = \rho \sum_{i \in [d]} \hat{\Sigma}_{i,i} / d$ and $\rho = 10^{-6}$. To approximate full correction, we use Algorithm 2 with GSL selection rule and implement the stopping rule from Remark 4.1 with, unless otherwise stated, $\alpha = 1$, $\beta = 10$ and $\tau = 10^{-5}$. We deliberately consider matrices of moderate dimension; this allows us to explore the regularisation paths of Glasso, compute sequential growths in full, and perform multiple repetitions of the considered experiments.

Remark 6.1. We consider the standard Glasso formulation (see Section 1) and use the GGlasso Python package [34] for computations. For a given matrix \mathbf{S} , we approximate the regularisation path of Glasso by discretising the interval $[0, \max_{i \neq j} |\mathbf{S}_{i,j}|]$; we use 100 uniformly-spaced values of the regularisation parameter. \triangleleft

Remark 6.2 (naive graph sequential growths). For $\mathbf{S} \in \mathcal{S}_{>0}^d$, we refer to the graph sequential growth induced by the ordering, in decreasing order, of the absolute values of the upper-diagonal entries of $\mathbf{Q} = \mathbf{S}^{-1}$ as the *precision-magnitude growth*; ties are broken randomly. Similarly, we define the *partial-correlation-magnitude growth* as the growth induced by the ordering of the absolute values of the upper-diagonal entries of the matrix with i, j entry $-\mathbf{Q}_{i,j} / (\mathbf{Q}_{i,i} \mathbf{Q}_{j,j})^{1/2}$. For short, the resulting growth procedures are referred to as Prec and PCorr, respectively. These naive growths are implemented for comparison purposes; they relate to thresholding-based approaches. \triangleleft

6.1 Synthetic example based on 494_bus

We consider the symmetric positive-definite matrix \mathbf{M}_0 defined by the 494_bus instance of the SuiteSparse Matrix Collection [7], where we extract the second 50×50 diagonal block of \mathbf{M}_0 , and denote the resulting matrix by \mathbf{M} . We normalise the matrix \mathbf{M}^{-1} (covariance to correlation), and use the resulting matrix Σ as true covariance. We generate random samples from \mathcal{N}_Σ of size n , and use these samples to perform graphical-model estimation. The sparsity pattern of $\Theta = \Sigma^{-1}$ is presented in Figure 1. The underlying graph has $d = 50$ vertices and 30 edges, and the values of the corresponding precisions and partial correlations are given in Figure 3. Note that all the partial correlations are non-negative.

We first compare the accuracy of the edge sets selected by Algorithm 3 with GSL, BBI and BFCI selection rules. We consider the sample sizes $n = 30, 90$ and 160 , and in each case perform 100 repetitions for GSL and BBI (that is, we generate 100 random samples from \mathcal{N}_Σ), and 10 repetitions for BFCI. Figure 1 shows the resulting graph-recovery ROC and precision-recall curves, the latter placing more emphasis on the accuracies achieved in the early stages of the extraction procedures; FP stands for false positive. We do not observe any notable differences between the considered selection rules, supporting the use of GSL or BBI selection rules as numerically efficient approximations of the BFCI rule.

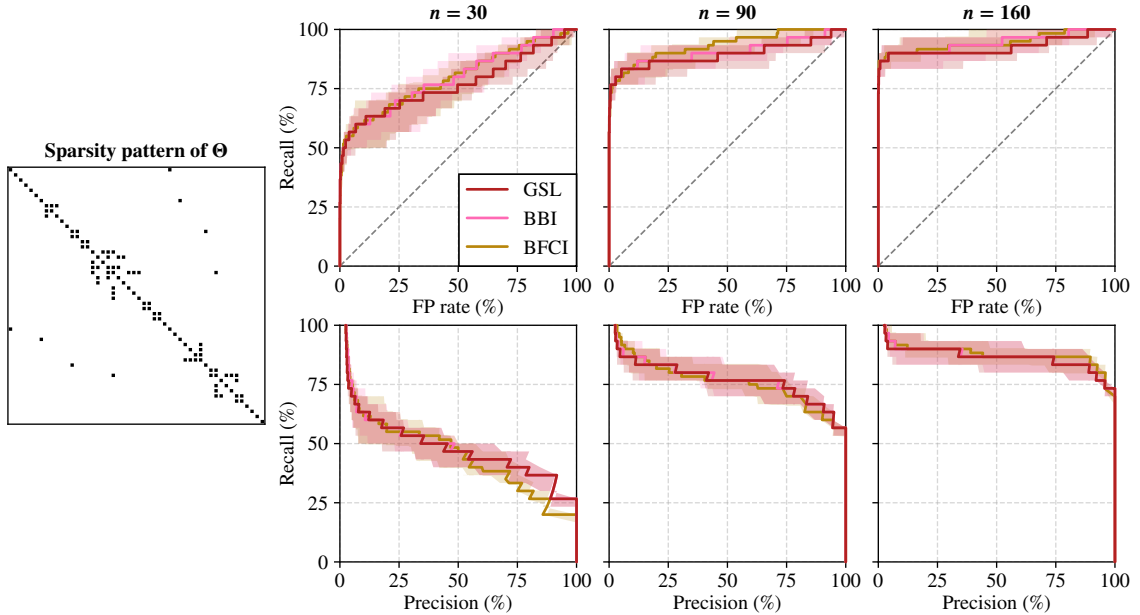


Figure 1: For the 494_bus example, ROC curves (top row) and precision-recall curves (bottom row) for the graphs for the sequential growths induced by the GSL, BBI and BFCI selection rules with approximate full correction. For each sample size, 100 repetitions are performed for GSL and BBI, and 10 for BFCI. The curves indicate the median accuracies, and the coloured regions the pointwise interdecile ranges. See Section 6.1.

Next, we compare the accuracy of the graphs recovered via GSL with the ones obtained via Glasso and the Prec and PCorr naive sequential growth procedures. We consider the same sample sizes $n = 30, 90$ and 160 , and perform 100 repetitions for each method. The results are presented in Figure 2, where we display both ROC and precision-recall curves. We observe that in the sparse regime, the best accuracies are systematically achieved by

GSL, Glasso catching up as the number of extracted edges increases. For $n = 30$, the first crossing between the GSL and Glasso median curves corresponds to a graph with 40 edges (recall that the number of true edges in this example is 30); for $n = 90$, the number of edges at crossing is 39, and 36 for $n = 160$. The GSL variant of Algorithm 3 also significantly outperforms Prec and PCorr in the early stages of the growth procedures.

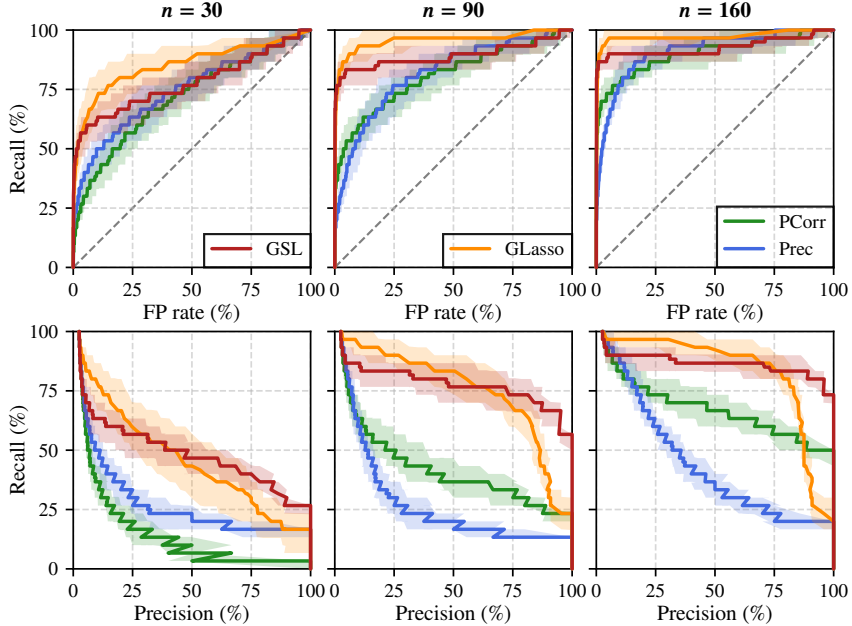


Figure 2: For the 494_bus example, ROC curves (top row) and precision-recall curves (bottom row) for the graphs recovered via GSL, Glasso, Prec and Pcorr. Sample sizes correspond to columns in the figure. The curves indicate the median accuracies over 100 repetitions and the coloured regions the pointwise interdecile ranges. See Section 6.1

To further illustrate the ability of our approach to reliably extract sparse models, we use GSL to extract graphs with $k = 30$ edges, which is the exact number of edges in the true underlying graph. We then assess the frequency of detection of the true edges, together with the distribution of the false positives (FPs). For comparison, we also extract graphs with $k = 30$ edges using Prec and PCorr. We set $n = 30$, and perform 500 repetitions. The results are presented in Figure 3. As already observed, GSL significantly outperforms Prec and PCorr in the considered regime. Despite the relatively small sample size, certain true edges are detected with high frequency, supporting the ability of GSL to efficiently leverage the information geometry of the problem. Also, with the exception of a few structural outliers, the false-positive distribution is remarkably uniform.

In a follow up experiment, we assess the positions in which edges are activated during the full GSL growth procedure; we call this position the *activation rank* of the respective edge. We use $n = 90$ and perform 500 repetitions, and order the edges according to their median activation rank. Figure 4 displays the rank box plots of the 55 foremost edges, together with the ones of all remaining true edges, of which there are only two. The results strongly support the ability of GSL to consistently identify relevant edges during the early stages of the growths. Apart from the edge (20, 22), whose signal is hardly distinguishable

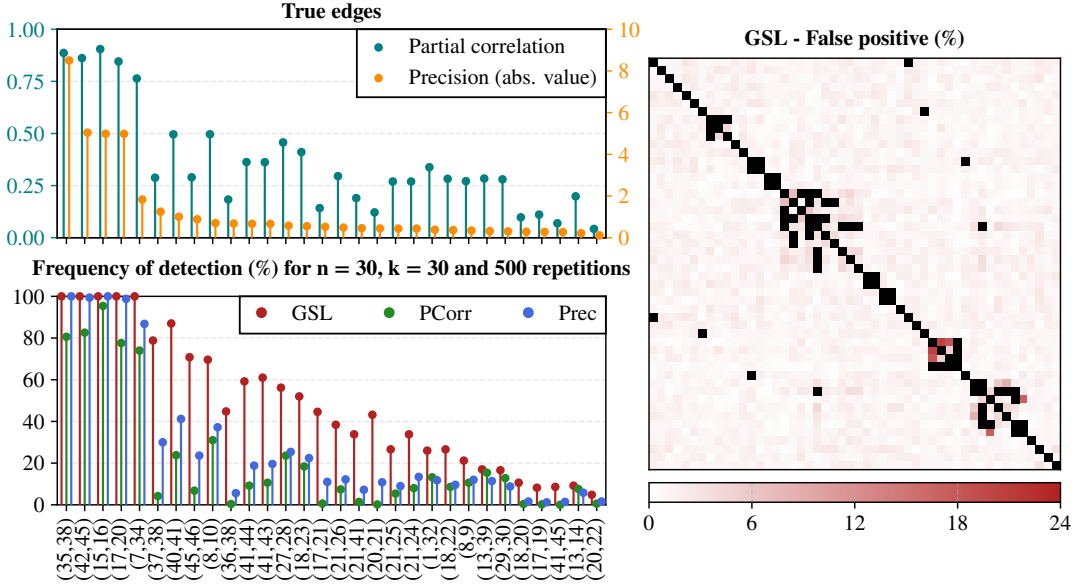


Figure 3: Graphical representation of the true partial correlations and precisions of the 30 true edges of the 494_bus example; the edges are ordered by decreasing absolute precision (top-left). For the sequential growth procedures GSL, Prec and PCorr, with $k = 30$ (that is, 30 edges are extracted), empirical frequency of detection of the true edges over 500 repetitions; the sample size is $n = 30$ (bottom-left). The empirical distribution of the false positives for GSL is also presented (right). See Section 6.1

from noise at $n = 90$ (see Figure 3), we observe a clear discrepancy between the activation-rank distributions of the true and false positives. Note that this type of investigations relates to the notion *stability selection* [27, 31]; see Section 6.3 for a further illustration.

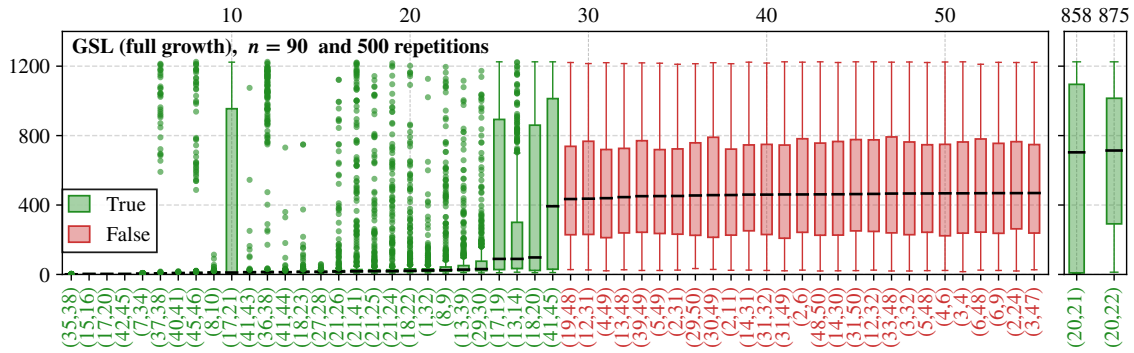


Figure 4: Distribution of the edge activation ranks under the full GSL growth procedure ($k = 1,225$) for the 494_bus example with $n = 90$ and 500 repetitions. The edges are ordered according to their median activation position (top horizontal axis). The 55 foremost edges are displayed (left), together with the remaining true edges (right). See Section 6.1.

To conclude this section, we investigate the impact of the precision of the approximate full corrections on the trade-off between computation cost and accuracy of the extraction. We consider the GSL variant of Algorithm 3 and a sample of size $n = 90$. As stopping pa-

rameters for the inner loop (see Remark 4.1), we use $\alpha = 1$ and $\beta = 10$, and consider three different values of τ , namely $\tau = 10^{-1}$, 10^{-3} and 10^{-5} , corresponding to a low, medium and high precision, respectively. For each value of τ , we record the evolution of the number of inner iterations in Algorithm 3 as a function of the number of outer iterations. In parallel, we record the evolution of the recalls of the recovered graphs. The results are presented in Figure 5. As expected, the number of inner iterations increases as τ decreases. Interestingly, similar graph-recovery performances are observed for the three considered values of τ , supporting the assertion that in the early stages of the growth process, relatively loose approximations of the full corrections can be used without jeopardising the accuracy of the recovered graphs.

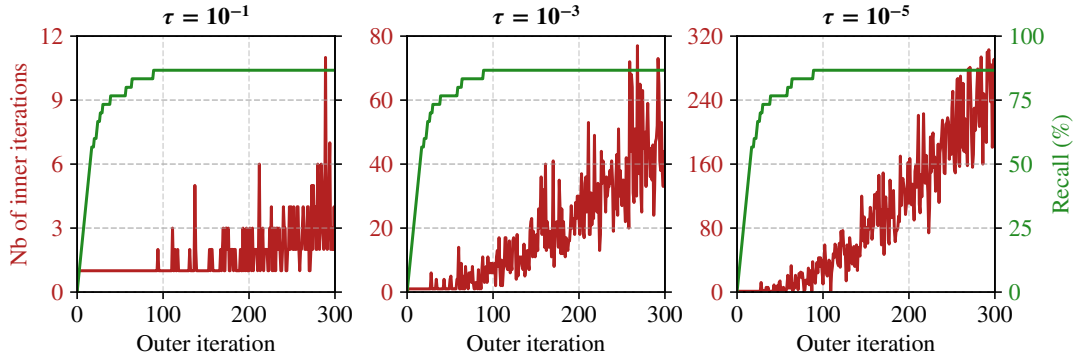


Figure 5: For a sample ($n = 90$) drawn in the setting of the 494_bus example, evolution of the number of inner iterations of the GSL variant of Algorithm 3 as a function of the number of outer iterations, for three different values of the threshold parameter τ , and with $\alpha = 1$ and $\beta = 10$ (see Remark 4.1). The evolution of the accuracy of the underlying graph-recovery process is also presented. See Section 6.1.

6.2 Fully-synthetic simulation study

We now assess the graph-recovery ability of the considered strategies across diverse scenarios. The considered graph structures are inspired by [2, 29] and presented in Figure 6. They are encoded by a symmetric base matrix $\mathbf{A} \in \mathcal{S}^d$, whose non-zero upper-diagonal entries are independent realisations of a random variable $Z = RU$, where R follows a Rademacher distribution, U a uniform distribution over $[0.5, 1.5]$, and with R and U independent; the diagonal of \mathbf{A} is set to 0. We next compute a solution $\mathbf{d}^* = (d_i^*)_{i \in [d]}$ to the semidefinite program

$$\text{minimise} \sum_{i \in [d]} d_i \text{ subject to } \mathbf{A} + \text{diag}(\mathbf{d}) \geq 0 \text{ and } \mathbf{d} \in \mathbb{R}_{\geq 0}^d;$$

we define $\mathbf{B} = \mathbf{A} + \text{diag}(\mathbf{d}^*) \in \mathcal{S}_{\geq 0}^d$ and set $\mathbf{M} = \mathbf{B} + \eta \mathbf{I}_d$, $\eta > 0$. We normalise the matrix \mathbf{M}^{-1} (covariance to correlation), and use the resulting matrix $\boldsymbol{\Sigma}$ as true covariance. The precision $\boldsymbol{\Theta} = \boldsymbol{\Sigma}^{-1}$ inherits the sparsity pattern from \mathbf{A} , and increasing η reduces the magnitude of the underlying true precision and partial correlations (we may interpret η as a signal-to-noise-ratio parameter). The considered graph structures are as follows.

- *Random*. The $m \in \mathbb{N}$ non-zero upper-diagonal entries of \mathbf{A} are selected uniformly at random over \mathcal{U} . We consider two cases: $m = 40$ and $m = 200$.
- *Clique*. The matrix \mathbf{A} is populated such that the precision matrix Θ consists of 5 diagonal blocks of order 10. The number of true edges is $m = 225$.
- *Hub*. The matrix \mathbf{A} is populated such that the resulting graph consists of 5 distinct hubs, each involving 10 nodes. The number of true edges is $m = 45$.

We use $d = 50$ and consider 3 sample sizes, namely $n = 30, 90$ and 160 , and in each case, we perform 100 repetitions for Glasso, GSL, BBI, Prec and Pcorr, and 10 for BFCI.

The results are presented in Figure 6 for $\eta = 0.25$ (strong-signal case), and Figure 7 for $\eta = 1$ (weak-signal case). They very much support the ability of the considered variants of Algorithm 3 to reliably identify relevant edges while limiting the number of false detections. Depending on the sparsity of the extracted graphs, the best median performances are systematically achieved by either Glasso or GSL, BBI or BFCI. In line with the 494_bus example, the most accurate sparse graphs are often the ones produced by Algorithm 3, except for Clique, where Glasso generally achieves a better accuracy. Interestingly, in the Clique example, we observe a relatively significant difference between the three variants of Algorithm 3, the best performances being achieved by BFCI, followed by BBI and GSL. Overall, the differences in accuracy between Glasso and the variants of Algorithm 3 are more significant for $\eta = 0.25$ than for $\eta = 1$. For the sparsest examples (that is, Random with $m = 40$ and Hub) with $\eta = 0.25$, the efficacy of the three variants of Algorithm 3 is remarkable, especially for $n = 90$ and $n = 160$.

6.3 Recovering a gene network: the Riboflavin data

The Riboflavin data relate to the genome of bacterias involved in the production of the riboflavin vitamin. The data set consists of $n = 71$ samples, reporting 4,088 gene expressions; it is available in the R package `hdi` [9]. Following [4, 22], we only consider the $d = 100$ genes with the highest empirical variances, and scale the data using the nonparanormal transformation [26]. We focus on the characterisation of sparse models (approximation of a non-necessarily sparse precision matrix), and more specially on the identification of gene clusters (gene-expression clustering). We use the GSL variant of Algorithm 3.

To gain insight into the range for which the generated graphs are likely to contain high proportions of true edges, we compute the edge-activation ranks induced by 500 random subsamples, without replacement, of size $\lfloor n/2 \rfloor = 35$ (see [31]), and order the edges according to their median activation position. In Figure 8, we present the activation-rank box plots for the 300 foremost edges. We do not observe a clear transition in the activation-rank distributions (such a transition is observed in Figure 4), so that a visual inspection does not rule out that the underlying true graph could contain more than 300 edges; observe however that the sample size is small, and that subsampling might induce artefacts. Sparse graphs containing up to approximately 100 edges appear likely to contain significant proportions of true edges.

In Figure 9, we present the graphs with $k = 40, 80$ and 120 edges defined by the subsampling-based activation ranks displayed in Figure 8; in each case, the edge set consists of the k foremost edges in terms of median activation rank. For comparison, we also

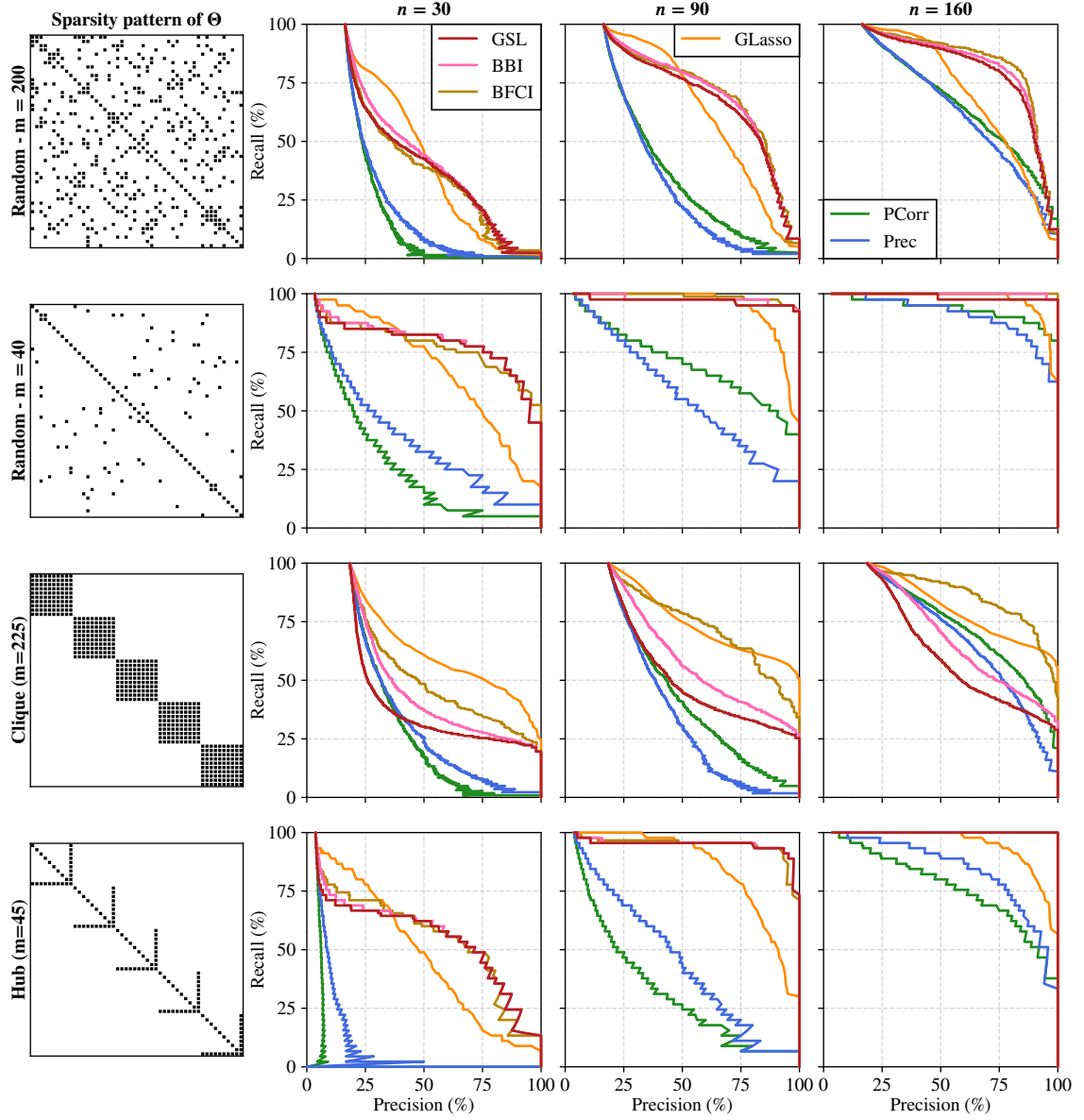
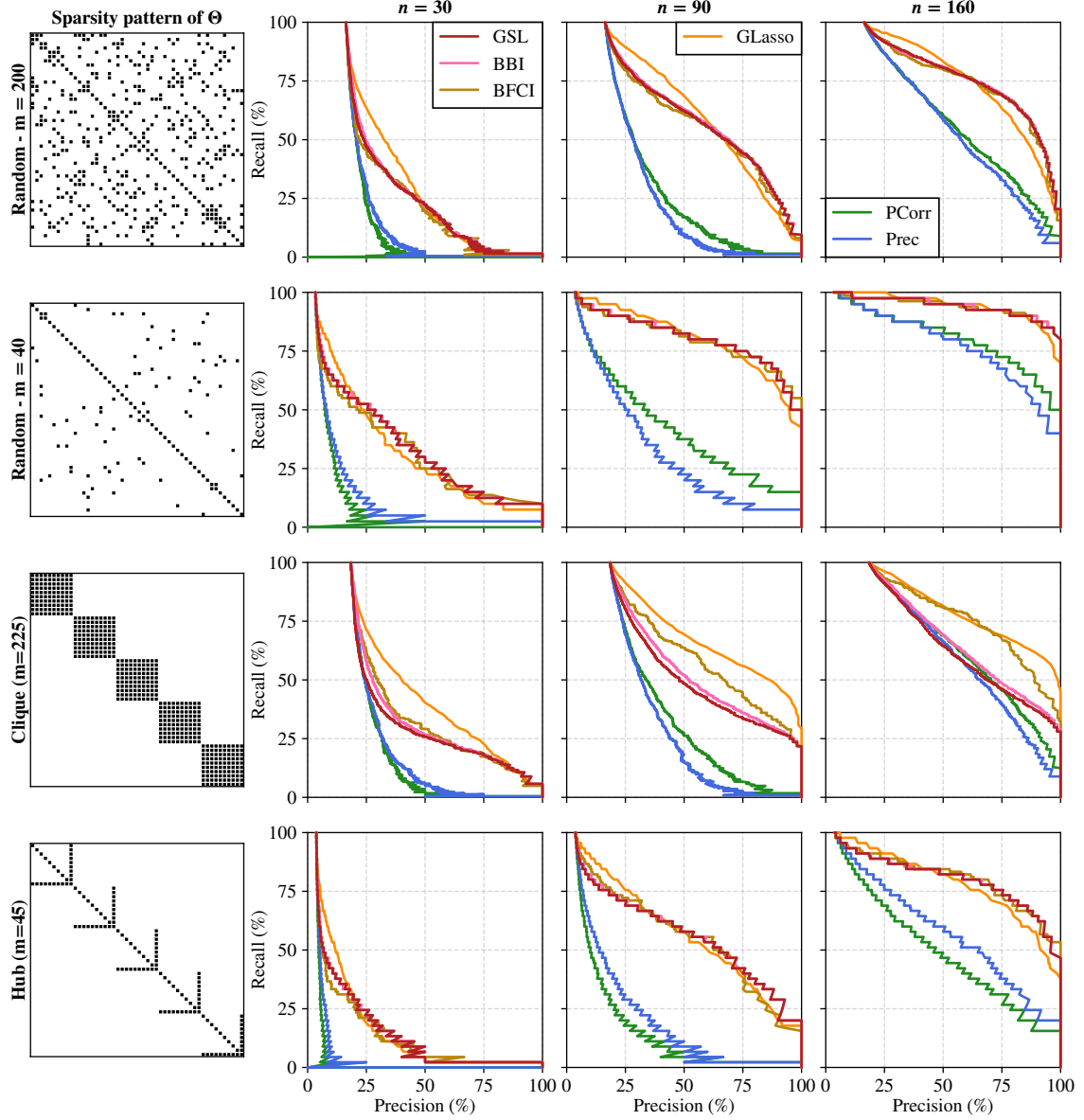


Figure 6: For the fully-synthetic examples with $\eta = 0.25$, precision-recall curves for the graphs recovered via GSL, BBI, BFCI, Glasso, Prec and Pcorr. The figure reads like a table, each row corresponding to a given example; for each example, three different sample sizes are considered. The curves indicate the median accuracies, over 10 repetitions for BFCI, and 100 repetitions for the other methods. See Section 6.2.


 Figure 7: Same setting as Figure 6, but with $\eta = 1$.

present in Figure 10, for the same values of k , the graphs produced by the GSL growth procedure applied to the full data set. The graphs reveal some intriguing patterns, illustrating the potential interest of the considered growth procedures for gene-expression clustering. Notably, the number of clusters can be easily adjusted by varying the edge-number parameter k . The graphs obtained for $k = 80$ share similarities with the one presented in [22], while the ones obtained for $k = 120$ appear relatively close to the one produced in [4]. Note that the graphs in Figure 9 require significantly more compute than their counterparts in Figure 10. More precisely, Figure 9 involves 500 full growths, against one partial growth for Figure 10.

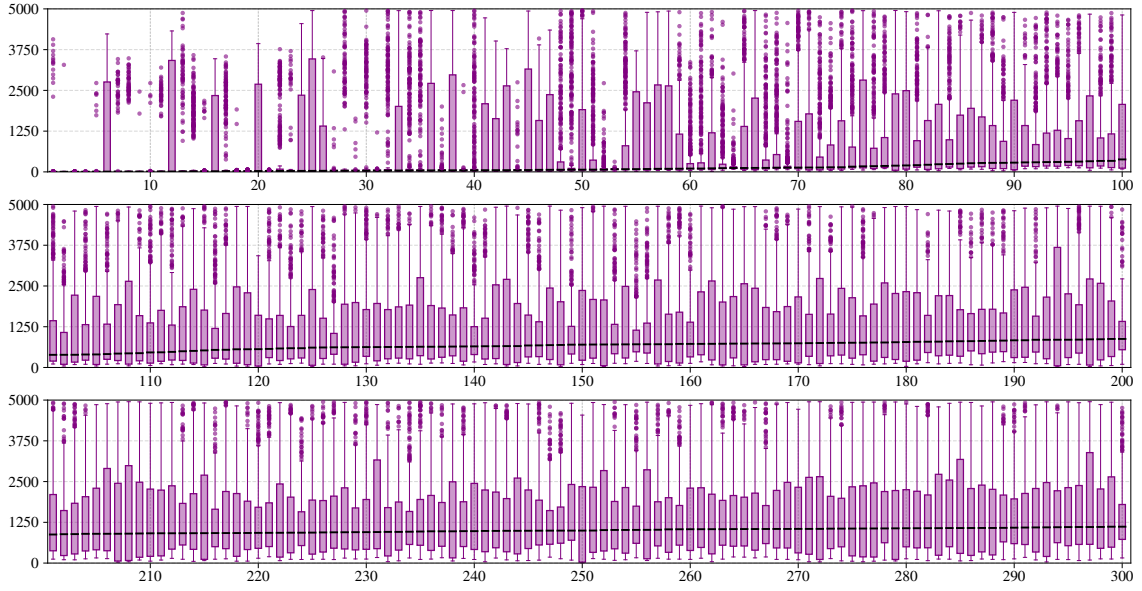


Figure 8: For the Riboflavin data and 500 random subsamples of size $[n/2] = 35$ (without replacement), distribution of the edge-activation ranks under the full GSL growth procedure ($k = 4,950$). The edges are ordered according to their median activation position; the 300 foremost edges are displayed. See Section 6.3.

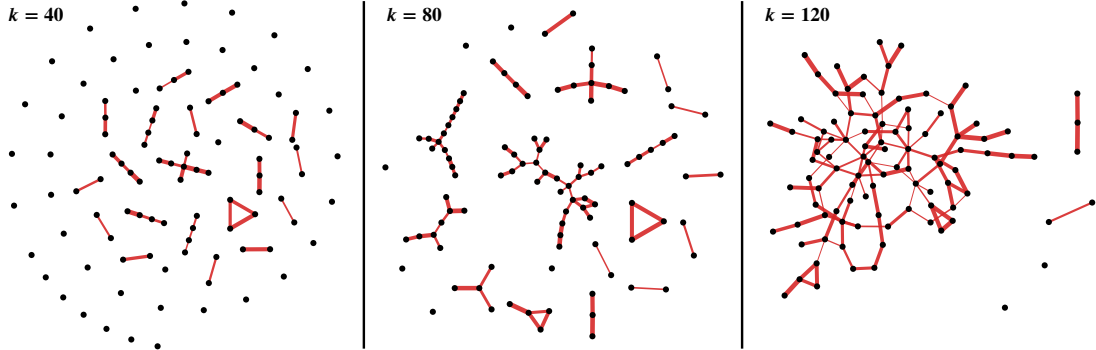


Figure 9: For the Riboflavin data, graphical representation of three graphs defined by subsampling-based activation ranks displayed in Figure 8. For a given value of k , the edge set of the graph consists of the k foremost edges in Figure 8. The width of the edges relates to their median rank, wider lines indicating lower median ranks. See Section 6.3.

7 Concluding discussion

We presented a class of regularisation-free approaches for Gaussian graphical inference based on the information-geometry-driven sequential growth of initially edgeless graphs. Leveraging the analogy between coordinate update and edge activation, we characterised the fully-corrective descents corresponding to information-optimal growths, and proposed numerically efficient strategies for their approximation. Our numerical experiments highlight the ability of the discussed procedures to reliably extract sparse models while limiting the number of false detections, providing an interesting complement to the existing

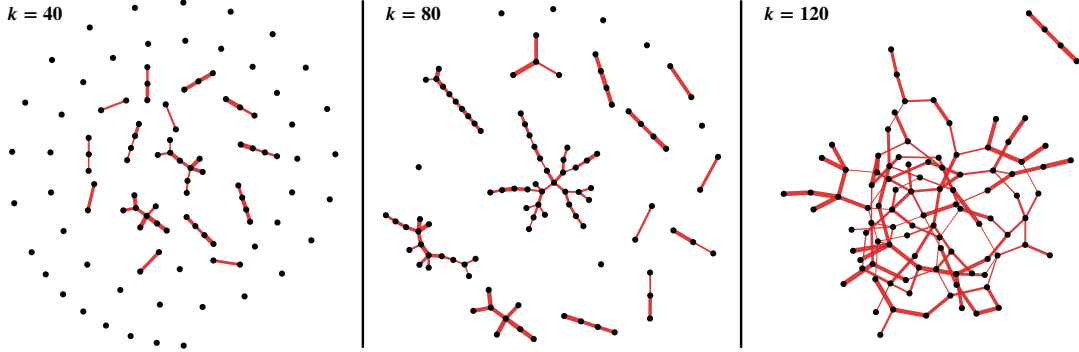


Figure 10: For the Riboflavin data, graphical representation of three graphs extracted by the GSL sequential growth procedure applied to the full data set. The width of the edges relates to their position in the growth process, wider lines indicating earlier activations. See Section 6.3

methodologies. Notably, the sequential nature of the discussed procedures offers an original diagnostic tool where the activation rank of the edges acts as a measure of their informational relevance, allowing for a nuanced assessment of the detected dependence structures. Aligning with the idea of stability selection, we also illustrated how the considered approaches can be combined with subsampling techniques to support the identification of relevant graphs.

Our investigations mostly focused on the graph-recovery ability of the proposed procedures, and follow-up studies could assess their relevance for parameter learning. The implementations of sequential growth procedures in constrained settings (such as total positivity, see for instance [23, 24]) could also offer an interesting avenue for future research. Finally, in the stability-selection framework, the design of relevant tests on the edge-activation ranks, together with the implementation of censoring techniques to account for partial growths, could help further improve the deployability and scalability of sequential-growth-based methodologies.

A Proofs and technical results

This section gathers proofs of the results stated in the main body of the paper. It also contains a technical result (Lemma A.1) used to prove the convergence of Algorithm 2. Recall that

$$\lambda_{\min}(\mathbf{Q}) \text{trace}(\mathbf{M}) \leq \text{trace}(\mathbf{QM}) \leq \lambda_{\max}(\mathbf{Q}) \text{trace}(\mathbf{M}), \quad (4)$$

for all $\mathbf{Q} \in \mathcal{S}^d$ and $\mathbf{M} \in \mathcal{S}_{\geq 0}^d$.

Proof of Lemma 2.1. Set $\mathbf{Q}^{-1} = \mathbf{A}^2$, with $\mathbf{A} \in \mathcal{S}_{>0}^d$; the strict convexity of $f_{\mathbf{S}}$ follows by observing that $D_{\mathbf{Q}}^2 f_{\mathbf{S}}(\mathbf{H}, \mathbf{H}) = \|\mathbf{A}\mathbf{H}\mathbf{A}\|_F^2 \geq 0$, $\mathbf{H} \in \mathcal{S}^d$, with equality if and only if $\mathbf{H} = 0$.

Assume that \mathbf{S} is invertible. We have $D_{\mathbf{Q}} f_{\mathbf{S}} = 0$ if and only if $\mathbf{Q} = \mathbf{S}^{-1}$, characterising the minimum of $f_{\mathbf{S}}$. Consider a sequence $(\mathbf{Q}_k)_{k \in \mathbb{N}} \subset \mathcal{S}_{>0}^d$. If $\lambda_{\max}(\mathbf{Q}_k) \rightarrow +\infty$, then from

(4), we have

$$f_S(\mathbf{Q}_k) \geq \lambda_{\min}(\mathbf{S})\lambda_{\max}(\mathbf{Q}_k) - d \log(\lambda_{\max}(\mathbf{Q}_k)) \rightarrow +\infty.$$

Also, as $\text{trace}(\mathbf{S}\mathbf{Q}_k) \geq 0$, $k \in \mathbb{N}$, we obtain that if $\det(\mathbf{Q}_k) \rightarrow 0$, then $f_S(\mathbf{Q}_k) \rightarrow +\infty$, proving the coercivity of f_S over $S_{>0}^d$.

Assume that \mathbf{S} is singular. Setting $\mathbf{S} = \text{diag}(\lambda_1, \dots, \lambda_p, 0, \dots, 0)$, with $p < d$ and $\lambda_i > 0$, and $\mathbf{Q}_k = \text{diag}(1/\lambda_1, \dots, 1/\lambda_p, k, \dots, k)$, $k \in \mathbb{N}$, we obtain

$$f_S(\mathbf{Q}_k) = p + \sum_{i=1}^p \log(\lambda_i) - (d-p)\log(k) \rightarrow -\infty \quad \text{as } k \rightarrow +\infty.$$

A similar argument applies to a general matrix \mathbf{S} via diagonalisation. \square

Proof of Lemma 2.2. We have $\nabla f_S(\mathbf{Q}_1) - \nabla f_S(\mathbf{Q}_2) = \mathbf{Q}_2^{-1} - \mathbf{Q}_1^{-1} = \mathbf{Q}_1^{-1}(\mathbf{Q}_1 - \mathbf{Q}_2)\mathbf{Q}_2^{-1}$. Both inequalities then follow from (4). \square

Proof of Lemma 2.3. The existence of a minimum follows from Lemma 2.1. We indeed have

$$\inf \{f_S(\mathbf{Q}) \mid \text{edge}(\mathbf{Q}) \subseteq \mathcal{E}\} = \inf \{f_S(\mathbf{Q}) \mid \text{edge}(\mathbf{Q}) \subseteq \mathcal{E} \text{ and } f_S(\mathbf{Q}) \leq f_S(\mathbf{Q}_{S,\emptyset})\},$$

and $\mathcal{K} = \{\mathbf{Q} \in S_{>0}^d \mid \text{edge}(\mathbf{Q}) \subseteq \mathcal{E} \text{ and } f_S(\mathbf{Q}) \leq f_S(\mathbf{Q}_{S,\emptyset})\}$ is convex and compact (intersection of a convex compact sublevel set of f_S with a linear subspace of S^d) and non-empty as $\mathbf{Q}_{S,\emptyset}$ is an element. Strict convexity of f_S ensures uniqueness. The zeroing of the entries of the gradient is a consequence of the openness of $\{\mathbf{Q} \in S_{>0}^d \mid \text{edge}(\mathbf{Q}) \subseteq \mathcal{E}\}$ in $\text{span}\{\mathbf{B}(i,j) \mid (i,j) \in \mathcal{D} \cup \mathcal{E}\}$. \square

Proof of Lemma 4.1. We have $\tilde{\mathbf{Q}} \in (\mathbf{Q} + \text{span}\{\mathbf{B}(i,j) \mid i,j \in I, i \leq j\})$, and a direct computation gives $\tilde{\mathbf{R}}^{-1} = \tilde{\mathbf{Q}}$. Moreover, we have $\tilde{\mathbf{Q}} > 0$ (that is, $\tilde{\mathbf{Q}}$ is symmetric positive-definite), since $\tilde{\mathbf{Q}}_{I^c, I^c} = \mathbf{Q}_{I^c, I^c} > 0$ and $\tilde{\mathbf{Q}}_{I, I} - \tilde{\mathbf{Q}}_{I, I^c}(\tilde{\mathbf{Q}}_{I^c, I^c})^{-1}\tilde{\mathbf{Q}}_{I^c, I} = (\mathbf{S}_{I, I})^{-1} > 0$, see e.g. [15, Theorem 7.7.7]. As $[\nabla f_S(\tilde{\mathbf{Q}})]_{I, I} = 0$, the optimality follows. A direct computation provides the value of the improvement $f_S(\mathbf{Q}) - f_S(\tilde{\mathbf{Q}})$. \square

Lemma A.1. Consider \mathbf{S} and $\mathbf{Q} \in S_{>0}^d$, and $\mathbf{H} \in S^d \setminus \{0\}$. For $\alpha \in \mathbb{R}$, set $\mathbf{Q}_\alpha = \mathbf{Q} + \alpha\mathbf{H}$. There exists α^* such that $\langle \nabla f_S(\mathbf{Q}_{\alpha^*}) \mid \mathbf{H} \rangle_F = 0$. Moreover, for any convex set $\mathcal{K} \subset S_{>0}^d$ such that \mathbf{Q} and $\mathbf{Q}_{\alpha^*} \in \mathcal{K}$ and $\lambda_{\min}(\mathcal{K}) > 0$, we have $|\alpha^*| \geq |\langle \nabla f_S(\mathbf{Q}) \mid \mathbf{H} \rangle_F| / (L\|\mathbf{H}\|_F^2)$ and $f_S(\mathbf{Q}) - f_S(\mathbf{Q}_{\alpha^*}) \geq \langle \nabla f_S(\mathbf{Q}) \mid \mathbf{H} \rangle_F^2 / (2L\|\mathbf{H}\|_F^2)$, with $L = 1/\lambda_{\min}^2(\mathcal{K})$.

Proof. The existence of α^* follows by convexity and coercivity of f_S (Lemma 2.1); observe that \mathbf{Q}_{α^*} is the unique minimum of f_S over the convex set $\{\mathbf{Q}_\alpha \mid \alpha \in \mathbb{R}\} \cap S_{>0}^d$ (exact line search from \mathbf{Q} along \mathbf{H}). By Cauchy-Schwartz and from the L -smoothness of f_S over \mathcal{K} (Lemma 2.2), we get

$$\begin{aligned} |\langle \nabla f_S(\mathbf{Q}) \mid \mathbf{H} \rangle_F| &= |\langle \nabla f_S(\mathbf{Q}) - \nabla f_S(\mathbf{Q}_{\alpha^*}) \mid \mathbf{H} \rangle_F| \\ &\leq \|\nabla f_S(\mathbf{Q}) - \nabla f_S(\mathbf{Q}_{\alpha^*})\|_F \|\mathbf{H}\|_F \leq |\alpha^*| L \|\mathbf{H}\|_F^2, \end{aligned}$$

providing the expected lower bound for $|\alpha^*|$.

From the L -smoothness of f_S , for all α such that $\mathbf{Q}_\alpha \in \mathcal{K}$, we have

$$f_S(\mathbf{Q}_\alpha) \leq f_S(\mathbf{Q}) + \alpha \langle \nabla f_S(\mathbf{Q}) \mid \mathbf{H} \rangle_F + \alpha^2 L \|\mathbf{H}\|_F^2 / 2 = \varphi(\alpha).$$

The minimum of the function φ over \mathbb{R} is reached at $\bar{\alpha} = -\langle \nabla f_S(\mathbf{Q}) | \mathbf{H} \rangle_F / (L \|\mathbf{H}\|_F^2)$. We thus have $|\alpha^*| \geq |\bar{\alpha}|$, and α^* and $\bar{\alpha}$ have same sign; the convexity of \mathcal{K} entails $\mathbf{Q}_{\bar{\alpha}} \in \mathcal{K}$. We obtain

$$f_S(\mathbf{Q}_{\alpha^*}) \leq f_S(\mathbf{Q}_{\bar{\alpha}}) \leq \varphi(\bar{\alpha}) = f_S(\mathbf{Q}) - \langle \nabla f_S(\mathbf{Q}) | \mathbf{H} \rangle_F^2 / (2L \|\mathbf{H}\|_F^2),$$

completing the proof. \square

Proof of Theorem 4.1. Consider $t \in \mathbb{N}$ and set $\mathbf{Q} = \mathbf{Q}^{(t-1)}$ and $\tilde{\mathbf{Q}} = \mathbf{Q}^{(t)}$. Also, denote by $\check{\mathbf{Q}}$ the iterate of an exact line search from $\mathbf{Q}^{(t-1)}$ along $\mathbf{B} = \mathbf{B}(i, j)^{(t)}$. By definition of $\tilde{\mathbf{Q}}$ and $\check{\mathbf{Q}}$, and from Lemma A.1 with $\mathcal{K} = \mathcal{K}_{0, \mathcal{E}}$, we have

$$f_S(\mathbf{Q}) - f_S(\tilde{\mathbf{Q}}) \geq f_S(\mathbf{Q}) - f_S(\check{\mathbf{Q}}) \geq \langle \nabla f_S(\mathbf{Q}) | \mathbf{B} \rangle_F^2 / (2L).$$

For $\mathcal{E} \subseteq \mathcal{U}$, define the semi-norm $\|\mathbf{M}\|_{F, \mathcal{E}}^2 = \sum_{(i, j) \in \mathcal{D} \cup \mathcal{E}} \langle \mathbf{M} | \mathbf{B}(i, j) \rangle_F^2$, $\mathbf{M} \in \mathcal{S}^d$, and denote the underlying semi-inner product accordingly. By definition of the GS rule, we have $\langle \nabla f_S(\mathbf{Q}) | \mathbf{B} \rangle_F^2 \geq \|\nabla f_S(\mathbf{Q})\|_{F, \mathcal{E}}^2 / m$, and so

$$f_S(\mathbf{Q}) - f_S(\tilde{\mathbf{Q}}) \geq \|\nabla f_S(\mathbf{Q})\|_{F, \mathcal{E}}^2 / (2Lm). \quad (5)$$

From the μ -strong convexity of f_S over $\mathcal{K}_{0, \mathcal{E}}$ and the existence of $\mathbf{Q}_{S, \mathcal{E}}$ (Lemmas 2.2 and 2.3), observing that $\mathbf{Q}_{S, \mathcal{E}}$ and \mathbf{Q} are both supported by $G = ([d], \mathcal{E})$, we have

$$f_S(\mathbf{Q}_{S, \mathcal{E}}) \geq f_S(\mathbf{Q}) + \langle \nabla f_S(\mathbf{Q}) | \mathbf{Q}_{S, \mathcal{E}} - \mathbf{Q} \rangle_{F, \mathcal{E}} + \mu \|\mathbf{Q}_{S, \mathcal{E}} - \mathbf{Q}\|_{F, \mathcal{E}}^2 / 2 = \psi(\mathbf{Q}_{S, \mathcal{E}}).$$

The map $\mathbf{M} \mapsto \psi(\mathbf{M})$, $\mathbf{M} \in \mathcal{S}^d$, is convex and minimal at $\bar{\mathbf{M}} = \mathbf{Q} - \nabla f_S(\mathbf{Q}) / \mu$, and so

$$f_S(\mathbf{Q}_{S, \mathcal{E}}) \geq \psi(\bar{\mathbf{M}}) = f_S(\mathbf{Q}) - \|\nabla f_S(\mathbf{Q})\|_{F, \mathcal{E}}^2 / (2\mu). \quad (6)$$

Combining (5) and (6), we get

$$f_S(\mathbf{Q}^{(t-1)}) - f_S(\mathbf{Q}^{(t)}) \geq \frac{\mu}{mL} (f_S(\mathbf{Q}^{(t-1)}) - f_S(\mathbf{Q}_{S, \mathcal{E}})), \quad t \in \mathbb{N}, \quad (7)$$

and the result follows. \square

Acknowledgements. The first author thankfully acknowledges financial support from the DTP 2224 Cardiff University (UKRI grant EP/W524682/1) at the School of Mathematics (project reference 2926088).

References

- [1] BANERJEE, O., EL GHAOUI, L., AND D'ASPREMONT, A. Model selection through sparse maximum likelihood estimation for multivariate Gaussian or binary data. *J. Mach. Learn. Res.* 9 (2008), 485–516.
- [2] BIEN, J., AND TIBSHIRANI, R. J. Sparse estimation of a covariance matrix. *Biometrika* 98, 4 (2011), 807–820.

- [3] BUBECK, S. Convex optimization: Algorithms and complexity. *Foundations and Trends® in Machine Learning* 8, 3-4 (11 2015), 231–357.
- [4] BÜHLMANN, P., KALISCH, M., AND MEIER, L. High-dimensional statistics with a view toward applications in biology. *Annu. Rev. Stat. Appl.* 1 (2014), 255–278.
- [5] BÜHLMANN, P., AND VAN DE GEER, S. *Statistics for high-dimensional data*. Springer Series in Statistics. Springer, Heidelberg, 2011.
- [6] CSISZÁR, I. *I*-divergence geometry of probability distributions and minimization problems. *Ann. Probability* 3 (1975), 146–158.
- [7] DAVIS, T. A., AND HU, Y. The University of Florida sparse matrix collection. *ACM Trans. Math. Software* 38, 1 (2011), Art. 1, 25.
- [8] DAWID, A. P. The geometry of proper scoring rules. *Ann. Inst. Statist. Math.* 59, 1 (2007), 77–93.
- [9] DEZEURE, R., BÜHLMANN, P., MEIER, L., AND MEINSHAUSEN, N. High-dimensional inference: confidence intervals, *p*-values and R-software `hdi`. *Statist. Sci.* 30, 4 (2015), 533–558.
- [10] DRTON, M., AND MAATHUIS, M. H. Structure learning in graphical modeling. *Annu. Rev. Stat. Appl.* 4 (2017), 365–393.
- [11] DRTON, M., AND PERLMAN, M. D. Model selection for Gaussian concentration graphs. *Biometrika* 91, 3 (2004), 591–602.
- [12] FRIEDMAN, J., HASTIE, T., AND TIBSHIRANI, R. Sparse inverse covariance estimation with the graphical lasso. *Biostatistics* 9, 3 (2008), 432–441.
- [13] HA, M. J., AND SUN, W. Partial correlation matrix estimation using ridge penalty followed by thresholding and re-estimation. *Biometrics* 70, 3 (2014), 765–773.
- [14] HØJSGAARD, S., AND LAURITZEN, S. L. On some algorithms for estimation in Gaussian graphical models. *Biometrika* 111, 4 (2024), 1201–1219.
- [15] HORN, R. A., AND JOHNSON, C. R. *Matrix analysis*, second ed. Cambridge University Press, Cambridge, 2013.
- [16] JANKOVÁ, J., AND VAN DE GEER, S. Confidence intervals for high-dimensional inverse covariance estimation. *Electron. J. Stat.* 9, 1 (2015), 1205–1229.
- [17] JANKOVÁ, J., AND VAN DE GEER, S. Inference in high-dimensional graphical models. In *Handbook of graphical models*, Chapman & Hall/CRC Handb. Mod. Stat. Methods. CRC Press, Boca Raton, FL, 2019, pp. 325–349.
- [18] JOG, V., AND LOH, P.-L. On model misspecification and KL separation for Gaussian graphical models. In *2015 IEEE International Symposium on Information Theory (ISIT)* (2015), IEEE, pp. 1174–1178.
- [19] KARIMI, H., NUTINI, J., AND SCHMIDT, M. Linear convergence of gradient and proximal-gradient methods under the Polyak-Lojasiewicz condition. In *Joint European Conference on Machine Learning and Knowledge Discovery in Databases* (2016), pp. 795–811.
- [20] KOKA, T., MACHKOUR, J., AND MUMA, M. False discovery rate control for Gaussian graphical models via neighborhood screening. In *2024 32nd European Signal Processing Conference (EUSIPCO)* (2024), pp. 2482–2486.
- [21] KULLBACK, S. *Information theory and statistics*. Dover Publications, Inc., Mineola, NY, 1997. Reprint of the second (1968) edition.
- [22] LASZKIEWICZ, M., FISCHER, A., AND LEDERER, J. Thresholded adaptive validation: Tuning the graphical lasso for graph recovery. In *Proc. Mach. Learn. Res.* (2021), vol. 130, pp. 1864–1872.

- [23] LAURITZEN, S., UHLER, C., AND ZWIERNIK, P. Maximum likelihood estimation in Gaussian models under total positivity. *Ann. Statist.* 47, 4 (2019), 1835–1863.
- [24] LAURITZEN, S., AND ZWIERNIK, P. Locally associated graphical models and mixed convex exponential families. *Ann. Statist.* 50, 5 (2022), 3009–3038.
- [25] LAURITZEN, S. L. *Graphical models*, vol. 17 of *Oxford Statistical Science Series*. The Clarendon Press, Oxford University Press, New York, 1996.
- [26] LIU, H., LAFFERTY, J., AND WASSERMAN, L. The nonparanormal: semiparametric estimation of high dimensional undirected graphs. *J. Mach. Learn. Res.* 10 (2009), 2295–2328.
- [27] LIU, H., ROEDER, K., AND WASSERMAN, L. Stability approach to regularization selection (StARS) for high dimensional graphical models. In *Adv. Neural Inf. Process. Syst.* (2010).
- [28] LIU, W. Gaussian graphical model estimation with false discovery rate control. *Ann. Statist.* 41, 6 (2013), 2948–2978.
- [29] MAZUMDER, R., AND HASTIE, T. The graphical lasso: new insights and alternatives. *Electron. J. Stat.* 6 (2012), 2125–2149.
- [30] MEINSHAUSEN, N., AND BÜHLMANN, P. High-dimensional graphs and variable selection with the lasso. *Ann. Statist.* 34, 3 (2006), 1436–1462.
- [31] MEINSHAUSEN, N., AND BÜHLMANN, P. Stability selection. *J. R. Stat. Soc. Ser. B Stat. Methodol.* 72, 4 (2010), 417–473.
- [32] NESTEROV, Y. Efficiency of coordinate descent methods on huge-scale optimization problems. *SIAM J. Optim.* 22, 2 (2012), 341–362.
- [33] NUTINI, J., SCHMIDT, M., LARADJI, I., FRIEDLANDER, M., AND KOEPKE, H. Coordinate descent converges faster with the Gauss-Southwell rule than random selection. In *Proc. Mach. Learn. Res.* (2015), vol. 37, pp. 1632–1641.
- [34] SCHAIFF, F., VLASOVETS, O., AND MÜLLER, C. L. GGlasso - a Python package for General Graphical Lasso computation. *Journal of Open Source Software* 6, 68 (2021), 3865.
- [35] SHUTTA, K. H., DE VITO, R., SCHOLTENS, D. M., AND BALASUBRAMANIAN, R. Gaussian graphical models with applications to omics analyses. *Stat. Med.* 41, 25 (2022), 5150–5187.
- [36] SPEED, T. P., AND KIIVERI, H. T. Gaussian Markov distributions over finite graphs. *Ann. Statist.* 14, 1 (1986), 138–150.
- [37] UHLER, C. Gaussian graphical models. In *Handbook of graphical models*, Chapman & Hall/CRC Handb. Mod. Stat. Methods. CRC Press, Boca Raton, FL, 2019, pp. 217–238.
- [38] VAN WIERINGEN, W. N., STAM, K. A., PEETERS, C. F. W., AND VAN DE WIEL, M. A. Updating of the Gaussian graphical model through targeted penalized estimation. *J. Multivariate Anal.* 178 (2020), 104621, 14.
- [39] WITTEN, D. M., FRIEDMAN, J. H., AND SIMON, N. New insights and faster computations for the graphical lasso. *J. Comput. Graph. Statist.* 20, 4 (2011), 892–900.
- [40] YUAN, M., AND LIN, Y. Model selection and estimation in the Gaussian graphical model. *Biometrika* 94, 1 (2007), 19–35.